Check for updates

Dual-comb spectroscopy with tailored spectral broadening in Si₃N₄ nanophotonics

ESTHER BAUMANN,[1,4,*] ELI V. HOENIG,[1] EDGAR F. PEREZ,[1] GABRIEL M. COLACION,[1] FABRIZIO R. GIORGETTA,[1,4] KEVIN C. COSSEL,[1] GABRIEL YCAS,[1,4] DAVID R. CARLSON,[2] DANIEL D. HICKSTEIN,[2] KARTIK SRINIVASAN,[3] SCOTT B. PAPP,[2,4] NATHAN R. NEWBURY,[1] AND IAN CODDINGTON[1]

[1]*NIST Applied Physics Division, Boulder, CO 80305, USA*
[2]*NIST Time and Frequency Division, Boulder, CO 80305, USA*
[3]*NIST Center for Nanoscale Science and Technology, Gaithersburg, MD 20899, USA*
[4]*Department of Physics, University of Colorado Boulder, Boulder, CO 80309, USA*
baumann@nist.gov

Abstract: Si₃N₄ waveguides, pumped at 1550 nm, can provide spectrally smooth, broadband light for gas spectroscopy in the important 2 μm to 2.5 μm atmospheric water window, which is only partially accessible with silica-fiber based systems. By combining Er⁺ fiber frequency combs and supercontinuum generation in tailored Si₃N₄ waveguides, high signal-to-noise dual-comb spectroscopy spanning 2 μm to 2.5 μm is demonstrated. Acquired broadband dual-comb spectra of CO and CO_2 agree well with database line shape models and have a spectral-signal-to-noise as high as $48/\sqrt{s}$, showing that the high coherence between the two combs is retained in the Si₃N₄ supercontinuum generation. The dual-comb spectroscopy figure of merit is $6 \times 10^6/\sqrt{s}$, equivalent to that of all-fiber dual-comb spectroscopy systems in the 1.6 μm band. based on these results, future dual-comb spectroscopy can combine fiber comb technology with Si₃N₄ waveguides to access new spectral windows in a robust non-laboratory platform.

1. Introduction

Frequency-comb spectroscopy can rival and exceed the signal-to-noise, speed, resolution and precision of traditional broadband spectroscopy [1–5]. Although comb spectroscopy has been shown with bandwidths over ~4700 cm⁻¹ (~140 THz) in several spectral regions [6–8], frequency-comb sources still lag behind traditional broadband thermal sources in spectral coverage. Spectral smoothness for comb systems is also a challenge as strong spectral variations can be difficult to remove from the final spectrum and may result in unusable spectral regions. While it is unlikely that any laser-based source will ever be as spectrally broad and smooth as traditional black-body sources, which include the sun, widespread adoption of comb-based spectroscopy may require the ability to generate spectrally smooth reasonably broadband light easily and flexibly across the spectrum. Moreover, to exploit coherent techniques, such as dual-comb spectroscopy, this light must maintain its coherence in both the temporal and spatial domains.

One attractive solution for generating broadband light in many spectral regions is spectral broadening in nanophotonic waveguides [9–19]. Nanophotonic waveguides have many advantages relative to traditional non-linear fibers, including compactness, high nonlinearity, control of the waveguide dispersion, broad transparency windows, and a small Raman coefficient providing high coherence [20]. One particularly promising material is silicon nitride (Si₃N₄, or written here as SiN), which has enabled spectral broadening in the visible, near-infrared, and mid-infrared [14–19]. SiN offers a high nonlinear index of $25 \times 10^{-19}\,\mathrm{m^2/W}$ in addition to a wide bandgap that eliminates two-photon absorption when pumped at telecommunications wavelengths [21]. Other nonlinear waveguide materials are also attractive but currently many lack the maturity of SiN, which can be fabricated into high

confinement waveguides at a very high yield [22], can also be obtained from commercial vendors and has long been an enabling material in the field of micro combs [23,24].

While, recently, much of the spectral broadening in nanophotonic waveguides has been performed with an eye towards molecular spectroscopy [11–14,16,18,19] and dual-comb spectroscopy in particular, there has only been one partial waveguide based dual-comb spectroscopy demonstration [25]. This demonstration employed spectral broadening in a silicon waveguide but for only one of the two combs and with low system coherence.

Here we demonstrate fully coherent, high-resolution dual-comb spectroscopy with SiN waveguides. We show that dual-comb spectroscopy spectra with quality factors rivaling the state-of-the-art [3] can indeed be obtained. We also demonstrate an important caveat, which is that single spatial mode operation must be ensured. With imperfect coupler design, higher order spatial modes, which are easily generated in these devices, will lead to strong and varying structure in the spectra, crippling the overall dual-comb spectroscopy performance. In this work we target the entire 2 μm to 2.5 μm atmospheric transmission window, which is of interest for space-based measurements of atmospheric gases including CO, CO_2, CH_4, NH_3, and N_2O [26,27]. This same atmospheric window is appropriate for detection of chemicals of interest to agricultural and industrial process monitoring including HF, HCN, NH_3, and acetylene. However, since this window extends beyond the transparency edge of silica, it cannot be fully accessed by broadening in nonlinear fiber optics. Previous dual-comb spectroscopy results using chromium-based solid-state lasers and thulium fiber based combs partially accessed this region but at the cost of complexity relative to mature erbium technology as well as a narrower spectral coverage [28–30]. Accessing this spectral region through the combination of highly reliable Er^+:fiber combs [31–33] and SiN waveguides is an attractive option.

2. Experimental setup

Figure 1(a) shows a sketch of the experimental setup. Two compact fiber frequency combs with 160 MHz repetition rates (differing by 133 Hz) are phase stabilized and amplified to generate 50 fs, 1.9 nJ pulses centered at 1560 nm, with an average power of 300 mW. This amplified output is collimated and focused with two aspheric lenses onto a SiN waveguide.

The SiN waveguides were fabricated at Ligentec [40], using deep-UV lithography and chemical etching. The waveguides have a rectangular cross-section, and inverse tapers at both edge facets, which expand the mode field diameter to ~3 μm, improving input coupling efficiency of the 1560 nm Er^+ comb light. The SiN core is surrounded by a SiO_2 cladding layer as shown in the cross-section in Fig. 1(b). The output spectrum is tuned by choosing the waveguide dimensions and launched power appropriately [17]. To cover the 2-2.5 μm water window with high power and low spectral ripple, waveguides with a height of 770 nm, widths of 1516 nm and 2020 nm and a length of 2.8 mm are chosen. Also, we tested waveguides with intermediate widths and they all offered very similar coverage in the targeted spectral band. All waveguides exhibit strong anomalous dispersion at the 1560 nm pump wavelength (D = 75 ps/nm/km, see Fig. 1(c)). When seeded with 1.9 nJ, these waveguides produce a supercontinuum spanning more than 120 THz while crucially providing very smooth continuous coverage throughout the desired spectral band. The total power in the generated spectra is 65 mW with 8.8 mW between 120 THz and 155 THz as measured with a thermal detector head after the collimating off-axis parabolic mirror.

After spectral broadening in the waveguide, the light is collimated with an off-axis parabolic mirror. The output spectra are spectrally filtered by a 1.8 μm optical long-pass filter to avoid spectral aliasing and detector saturation and directed to a gas cell. The dual-comb spectroscopy signal is detected with an extended InGaAs photodiode followed by a 100 MHz transimpedance amplifier and a digitizer. The digitized time-domain interferograms are then phase corrected and co-added in real-time in a field programmable gate array (FPGA) [34].

Once a minute (every 8000 interferograms), a coadded interferogram is transferred from the FPGA to a computer and Fourier transformed to obtain a magnitude spectrum.
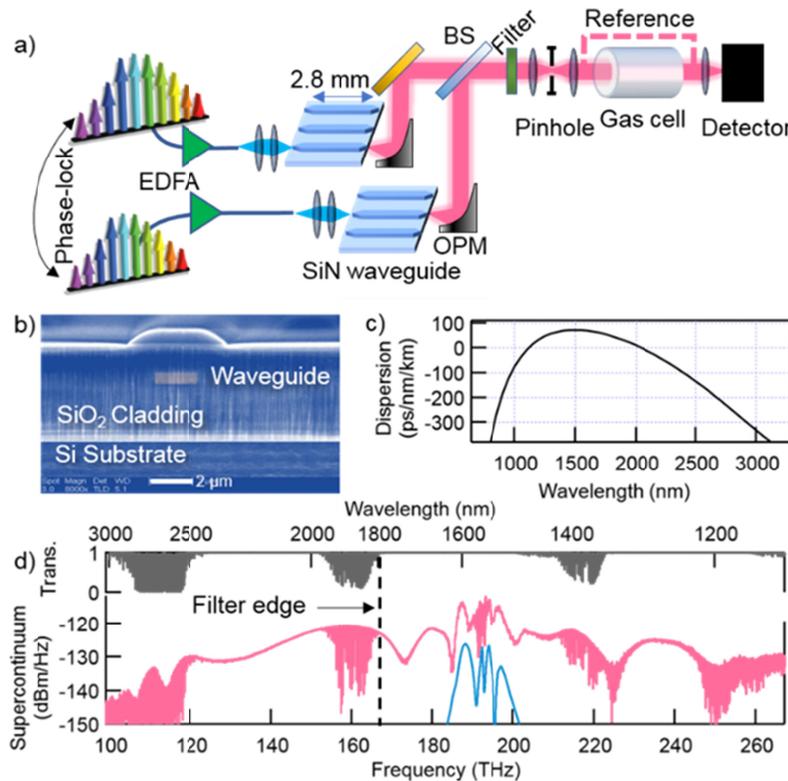

Fig. 1. Overview. a) Experimental setup. Two mutually coherent, self-referenced fiber laser frequency combs are amplified in an Er[+]-doped fiber amplifier (EDFA) and then focused into the waveguides with aspheric lenses. The supercontinuum output is collimated by an off-axis parabolic mirror (OPM), combined on a CaF_2 beam splitter (BS), directed through a 1.8 μm optical long-pass filter, spatially filtered with a 10 μm diameter pinhole, and finally transmitted through a 0.75 m gas cell filled with CO_2 and CO. A reference background spectrum is acquired over the labelled reference path sequentially after bypassing the cell via flip-mirrors. b) Scanning electron microscopy cross section of a non-tapered waveguide facet suspended in SiO_2 showing the waveguide dimensions. In the experiment, tapered waveguides are used for increased coupling efficiency. c) Calculated waveguide dispersion for a waveguide with a width of 2000 nm and a thickness of 770 nm. d) SiN generated supercontinuum (pink) and the input spectrum (blue), measured with an FTIR, as well as modelled transmission across a 2 m open-air path at 0.5% water (grey).

3. Dual-comb spectroscopy with waveguide broadened light

Figure 2(a) illustrates the challenges and strengths of spectral broadening in waveguides. While spectral coverage is easily obtained, these waveguides support higher order spatial modes which can interfere to create a strong noise-like structure as seen in Fig. 2(a) (green trace). Simulations suggest that these modes are excited in the waveguide, but they could also be driven by facet surface roughness or imperfect taper design. When the two combs are spatially combined these modes lead to strong inter-mode beating. Moreover, this structure varies over time and spatially across the beam front and cannot be easily removed using a reference spectrum. Fortunately, this structure can be strongly suppressed with spatial filtering after the waveguide, although, at the cost of optical power. Here we use a 10 μm diameter pinhole, which roughly matches the input beam's first Airy disc $1/e^2$-diameter of 8 μm, given by the focusing lens. For our system the associated loss is 7 dB, which is

dominated by the mismatch between the 12.7 mm diameter free-space beam and the 7.6 mm clear aperture focusing lens used in front of the pinhole, leaving only mW power levels to investigate the gas cell. Future studies that utilize nanophotonic waveguides for dual-comb spectroscopy may wish to implement tapered regions that more strongly suppress higher-order modes. Longer wavelengths may also be less affected.
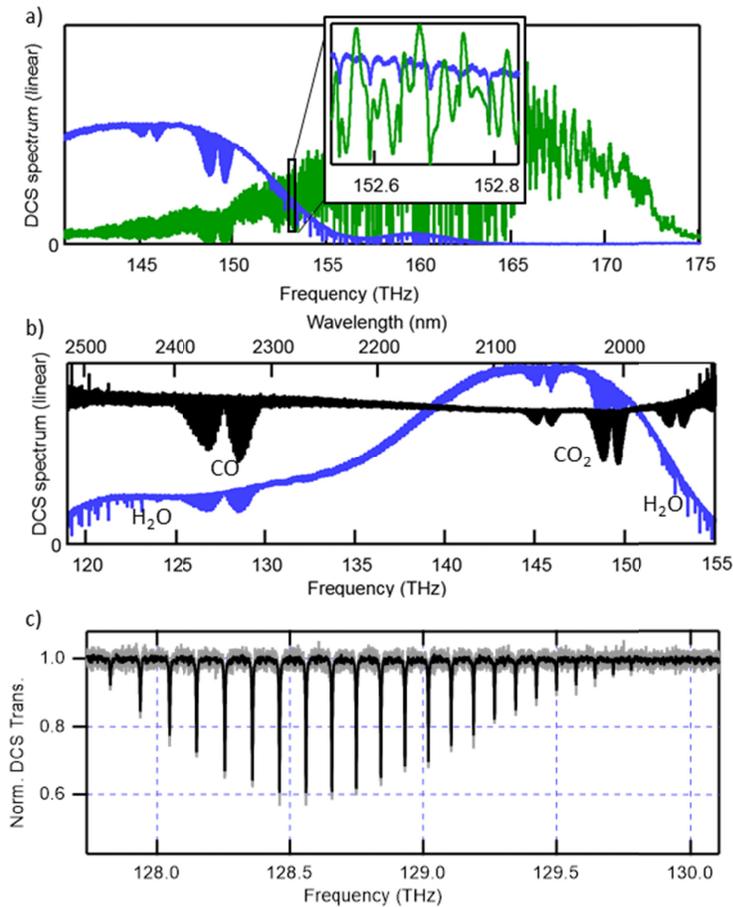

Fig. 2. Dual-comb spectroscopy spectra (1-minute long measurements, 160 MHz resolution). a) Without pinhole (green) and with pinhole preventing multimode interference (blue). The spectral coverage between the measurements varies due to different input power and input coupling. The narrow absorption features arise from CO_2 and water. The inset shows part of the spectrum where the signal-to-noise ratio (SNR) for the two measurements was comparable. b) Dual-comb spectroscopy spectra after spatial filtering with a pinhole (blue trace) and after additional normalization with the reference spectrum (black trace). CO_2 and CO absorption features from the gas cell are clearly visible. c) Detail of the normalized spectrum around the CO band. Both the fully resolved spectrum (grey trace, 160 MHz resolution) and a smoothed spectrum (black trace, 1.3 GHz resolution) show no baseline structure.

After spatial filtering, the dual-comb spectroscopy spectrum in Fig. 2(b) (blue trace) exhibits remaining structure from the comb spectra as well as a 26 GHz etalon fringe originating from the 2.8 mm long SiN waveguides. This structure can be suppressed by normalizing the measurement through the cell with a background reference spectrum acquired by bypassing the cell via flip-mirrors (black trace).

To characterize the performance of the optimized system, we examine transitions of CO $(2 \leftarrow 0)$ and CO_2 $(20011/20012/20013 \leftarrow 00001)$ in a 0.75 m long single-pass cell filled with

5.6% CO_2, 1.7% CO and 92.7% air to 840 mbar. After removing a remaining slowly varying residual spectral variation with a 4th order polynomial, we fit the CO and the CO_2 bands from the dual-comb spectroscopy measurement to a model based on Hitran 2016 [35] using gas concentrations and temperature as fit parameters, see Fig. 3(a). The white noise floor increases towards the edges of the normalized spectrum because of the reduced light intensity. The difference between fitted model and measurement is mostly flat with a standard deviation of 0.01 (as taken over the whole fitted spectral range), showing good agreement between measurement and model. An expanded view in Figs. 3(b) and 3(c) compares model and measurement for individual CO and CO_2 lines. While model and measurement match well, the difference shows some structure which we attribute to small inaccuracies in the Hitran 2016 database as well as to deviations from the Voigt lineshape [36].
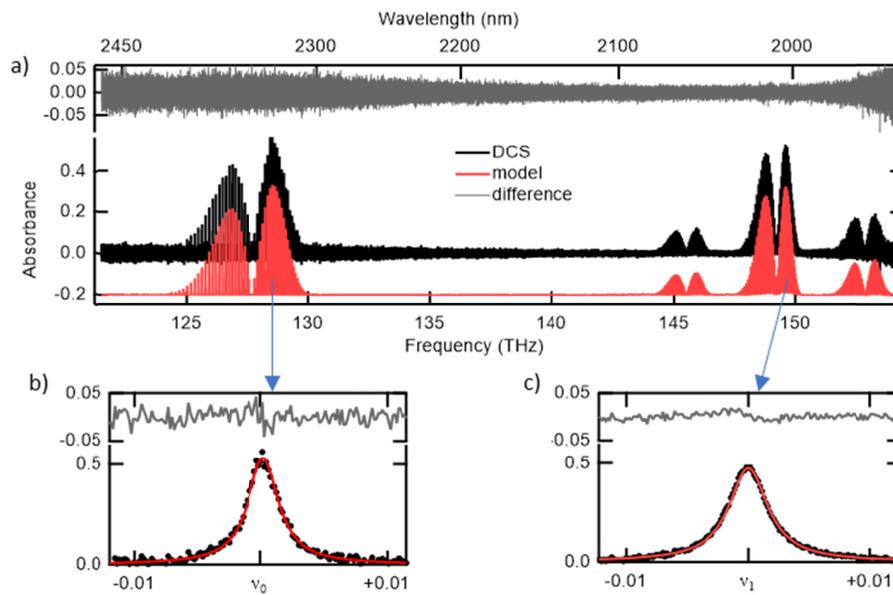

Fig. 3. Comparison between measurement and model at the combs' native 160 MHz resolution: a) Molecular absorbance from a 1-minute long dual-comb spectroscopy measurement (black) and from a fitted model based on Hitran 2016 (red) offset for clarity, along with their difference (grey). Expanded view of b) one CO absorption line at ν_0 = 128.559400 THz and c) one CO_2 line at ν_1 = 148.830794 THz.

4. Noise discussion

The peak spectral signal-to-noise ratio (SNR) of the raw 160 MHz tooth-resolved spectrum (blue trace in Fig. 2(b)) is $48/\sqrt{s}$ around 146 THz. However, for broadband spectral sources like frequency combs, the bandwidth and number of resolved points are equally important metrics. Following [37], we calculate a figure of merit defined as the product of the number of resolved spectral elements and average spectral SNR for the 160 MHz resolution spectra, normalized by the square root of the acquisition time. The entire dual-comb spectroscopy spectrum covers ~40 THz with 250,000 spectral elements and has an average SNR of 190 for a 60-second-long acquisition, resulting in a figure of merit of $6 \times 10^6 /\sqrt{s}$, which is comparable to previously reported all-fiber HNLF-broadened dual-comb spectroscopy in the near-infrared, which has a figure of merit of $7 \times 10^6 /\sqrt{s}$ [31]. This high SNR demonstrates that the supercontinuum generation process in the SiN waveguides does not significantly degrade the overall comb coherence or dual-comb spectroscopy performance. The spectral

SNR is calculated from the residual (difference between model and measurement) in Fig. 3(a) after high pass filtering to remove remaining etalon fringes.

Figure 4(a) compares the relative intensity noise (RIN) of the amplified comb light and the supercontinuum after the 1.8 μm optical long-wave filter. Even with the significant spectral broadening the supercontinuum light sees only a 2-3 dB increase in RIN at most frequencies relative to the input comb pulses. In comparison, similar efforts using highly non-linear silica fiber [38] suffered larger increases in RIN (5-10 dB) despite only broadening to 2.2 μm. The lower RIN seen here is attributed to the small Raman coefficient in SiN. Figure 4(b) shows the SNR of the transmission spectra as function of optical power levels measured with a powermeter placed in front of the photodiode. The optical power was decreased with an adjustable aperture. At optical powers above 300 μW the SNR becomes RIN limited for our system. Thus, increasing the optical power level on the photodiode beyond 300 μW does not further improve the SNR [37]. Detector non-linearities start to manifest themselves at power levels of around 400 μW, hence care was taken to perform dual-comb spectroscopy measurement with 300 μW of optical power on the detector.
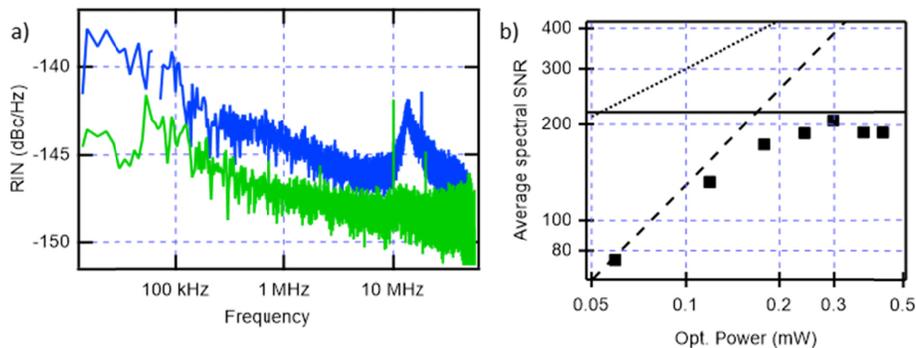

Fig. 4. Relative intensity noise (RIN) measurements of the amplified comb light (green) and the SiN-waveguide broadened supercontinuum after the 1.8 μm filter (blue). The noise peak at 13 MHz arises from the non-linear amplification of a wake-mode instability specific to this oscillator design [39]. b) Averaged spectral SNR for a 60-second-long measurement as a function of optical power on the detector (squares). The dashed line is the calculated detector-noise limited SNR for a $12 \, pW / \sqrt{Hz}$ noise-equivalent-power (NEP), the solid line is the RIN limited SNR (calculated for −140 dBc/Hz), and the dotted line is the calculated shot-noise limited SNR. Note that at an optical power of 300 μW, the shot-noise is equivalent to a noise level of $9 \, pW / \sqrt{Hz}$, below the $12 \, pW / \sqrt{Hz}$ NEP of the detector.

5. Conclusions

To conclude, we have demonstrated dual-comb spectroscopy using supercontinua generated in SiN waveguides seeded by compact Er$^+$:fiber combs. After spatial filtering with a pinhole, a smooth spectral shape is obtained. In future systems, improved waveguide designs, in particular different adiabatic coupling tapers for the input and output light, should obviate the need for a pinhole leading to an even more compact, robust system. High spectral fidelity is confirmed by the excellent agreement between measured CO and CO_2 line shapes and the Hitran model. The high SNR of the acquired dual-comb spectroscopy spectra show that the coherence of the underlying Er$^+$:fiber combs is retained, and the RIN is not significantly increased in the broadening process. The achieved figure of merit of $6 \times 10^6 \, /\sqrt{s}$ is comparable to all-fiber systems. Here, we targeted the spectral region from 2 μm to 2.5 μm, an important atmospheric window that is not accessible with silica-based fiber systems. Looking forward, the same configuration could be used to access other spectral regions through the near-infrared and potentially into the mid-infrared.

Funding

Acknowledgements

References

1. F. Adler, M. J. Thorpe, K. C. Cossel, and J. Ye, "Cavity-enhanced direct frequency comb spectroscopy: technology and applications," Annu. Rev. Anal. Chem. (Palo Alto, Calif.) **3**(1), 175–205 (2010).
2. A. Schliesser, N. Picqué, and T. W. Hänsch, "Mid-infrared frequency combs," Nat. Photonics **6**(7), 440–449 (2012).
3. I. Coddington, N. Newbury, and W. Swann, "Dual-comb spectroscopy," Optica **3**(4), 414–426 (2016).
4. K. C. Cossel, E. M. Waxman, I. A. Finneran, G. A. Blake, J. Ye, and N. R. Newbury, "Gas-phase broadband spectroscopy using active sources: progress, status, and applications," J. Opt. Soc. Am. B **34**(1), 104–129 (2017).
5. T. Ideguchi, "Dual-Comb Spectroscopy," Opt. Photonics News **28**(1), 32–39 (2017).
6. A. V. Muraviev, V. O. Smolski, Z. E. Loparo, and K. L. Vodopyanov, "Massively parallel sensing of trace molecules and their isotopologues with broadband subharmonic mid-infrared frequency combs," Nat. Photonics **12**(4), 209–214 (2018).
7. S. Okubo, K. Iwakuni, H. Inaba, K. Hosaka, A. Onae, H. Sasada, and F.-L. Hong, "Ultra-broadband dual-comb spectroscopy across 1.0–1.9 µm," Appl. Phys. Express **8**(8), 082402 (2015).
8. A. S. Kowligy, A. Lind, D. D. Hickstein, D. R. Carlson, H. Timmers, N. Nader, F. C. Cruz, G. Ycas, S. B. Papp, and S. A. Diddams, "Mid-infrared frequency comb generation via cascaded quadratic nonlinearities in quasi-phase-matched waveguides," Optics Letters **43**(8) 1678-1681 (2018).
9. M. A. Foster, A. C. Turner, M. Lipson, and A. L. Gaeta, "Nonlinear optics in photonic nanowires," Opt. Express **16**(2), 1300–1320 (2008).
10. D. D. Hickstein, H. Jung, D. R. Carlson, A. Lind, I. Coddington, K. Srinivasan, G. G. Ycas, D. C. Cole, A. Kowligy, C. Fredrick, S. Droste, E. S. Lamb, N. R. Newbury, H. X. Tang, S. A. Diddams, and S. B. Papp, "Ultrabroadband supercontinuum generation and frequency-comb stabilization using on-chip waveguides with both cubic and quadratic nonlinearities," Phys. Rev. Appl. **8**(1), 014025 (2017).
11. D. Yoon Oh, K. Y. Yang, C. Fredrick, G. Ycas, S. A. Diddams, and K. J. Vahala, "Coherent ultra-violet to near-infrared generation in silica ridge waveguides," Nat. Commun. **8**, 13922 (2017).
12. B. Kuyken, T. Ideguchi, S. Holzner, M. Yan, T. W. Hänsch, J. Van Campenhout, P. Verheyen, S. Coen, F. Leo, R. Baets, G. Roelkens, and N. Picqué, "An octave-spanning mid-infrared frequency comb generated in a silicon nanophotonic wire waveguide," Nat. Commun. **6**(1), 6310 (2015).
13. N. Singh, D. D. Hudson, Y. Yu, C. Grillet, S. D. Jackson, A. Casas-Bedoya, A. Read, P. Atanackovic, S. G. Duvall, S. Palomba, B. Luther-Davies, S. Madden, D. J. Moss, and B. J. Eggleton, "Midinfrared supercontinuum generation from 2 to 6 µm in a silicon nanowire," Optica **2**(9), 797–802 (2015).
14. A. R. Johnson, A. S. Mayer, A. Klenner, K. Luke, E. S. Lamb, M. R. E. Lamont, C. Joshi, Y. Okawachi, F. W. Wise, M. Lipson, U. Keller, and A. L. Gaeta, "Octave-spanning coherent supercontinuum generation in a silicon nitride waveguide," Opt. Lett. **40**(21), 5117–5120 (2015).
15. J. W. Choi, G. F. R. Chen, D. K. T. Ng, K. J. A. Ooi, and D. T. H. Tan, "Wideband nonlinear spectral broadening in ultra-short ultra - silicon rich nitride waveguides," Sci. Rep. **6**(1), 27120 (2016).
16. M. A. G. Porcel, F. Schepers, J. P. Epping, T. Hellwig, M. Hoekman, R. G. Heideman, P. J. M. van der Slot, C. J. Lee, R. Schmidt, R. Bratschitsch, C. Fallnich, and K.-J. Boller, "Two-octave spanning supercontinuum generation in stoichiometric silicon nitride waveguides pumped at telecom wavelengths," Opt. Express **25**(2), 1542–1554 (2017).
17. D. R. Carlson, D. D. Hickstein, A. Lind, S. Droste, D. Westly, N. Nader, I. Coddington, N. R. Newbury, K. Srinivasan, S. A. Diddams, and S. B. Papp, "Self-referenced frequency combs using high-efficiency silicon-nitride waveguides," Opt. Lett. **42**(12), 2314–2317 (2017).
18. D. Grassani, E. Tagkoudi, H. Guo, C. Herkommer, T. J. Kippenberg, and C.-S. Brès, "Highly efficient 4 micron light generation through fs-fiber laser driven supercontinuum in Si3N4 waveguides," ArXiv180606633 Phys. (2018).
19. H. Guo, C. Herkommer, A. Billat, D. Grassani, C. Zhang, M. H. P. Pfeiffer, W. Weng, C.-S. Brès, and T. J. Kippenberg, "Mid-infrared frequency comb via coherent dispersive wave generation in silicon nitride nanophotonic waveguides," Nat. Photonics **12**(6), 330–335 (2018).
20. A. Klenner, A. S. Mayer, A. R. Johnson, K. Luke, M. R. E. Lamont, Y. Okawachi, M. Lipson, A. L. Gaeta, and U. Keller, "Gigahertz frequency comb offset stabilization based on supercontinuum generation in silicon nitride waveguides," Opt. Express **24**(10), 11043–11053 (2016).
21. D. T. H. Tan, K. J. A. Ooi, and D. K. T. Ng, "Nonlinear optics on silicon-rich nitride—a high nonlinear figure of merit CMOS platform [Invited]," Photon. Res. **6**(5), B50–B66 (2018).

22. M. H. P. Pfeiffer, A. Kordts, V. Brasch, M. Zervas, M. Geiselmann, J. D. Jost, and T. J. Kippenberg, "Photonic Damascene process for integrated high-Q microresonator based nonlinear photonics," Optica **3**(1), 20–25 (2016).

23. T. J. Kippenberg, A. L. Gaeta, M. Lipson, and M. L. Gorodetsky, "Dissipative Kerr solitons in optical microresonators," Science **361**, eaan8083 (2018).

24. T. J. Kippenberg, R. Holzwarth, and S. A. Diddams, "Microresonator-based optical frequency combs," Science **332**(6029), 555–559 (2011).

25. N. Nader, D. L. Maser, F. C. Cruz, A. Kowligy, H. Timmers, J. Chiles, C. Fredrick, D. A. Westly, S. W. Nam, R. P. Mirin, J. M. Shainline, and S. Diddams, "Versatile silicon-waveguide supercontinuum for coherent mid-infrared spectroscopy," APL Photonics **3**(3), 036102 (2018).

26. H. Bovensmann, J. P. Burrows, M. Buchwitz, J. Frerick, S. Noël, V. V. Rozanov, K. V. Chance, and A. P. H. Goede, "SCIAMACHY: mission objectives and measurement modes," J. Atmos. Sci. **56**(2), 127–150 (1999).

27. G. Ehret, C. Kiemle, M. Wirth, A. Amediek, A. Fix, and S. Houweling, "Space-borne remote sensing of CO2, CH4, and N2O by integrated path differential absorption lidar: a sensitivity analysis," Appl. Phys. B **90**(3-4), 593–608 (2008).

28. B. Bernhardt, E. Sorokin, P. Jacquet, R. Thon, T. Becker, I. T. Sorokina, N. Picqué, and T. W. Hänsch, "Mid-infrared dual-comb spectroscopy with 2.4 μm Cr2+:ZnSe femtosecond lasers," Appl. Phys. B **100**(1), 3–8 (2010).

29. R. Liao, Y. Song, W. Liu, H. Shi, L. Chai, and M. Hu, "Dual-comb spectroscopy with a single free-running thulium-doped fiber laser," Opt. Express **26**(8), 11046–11054 (2018).

30. M. I. Kayes, N. Abdukerim, A. Rekik, and M. Rochette, "Free-running mode-locked laser based dual-comb spectroscopy," Opt. Lett. **43**(23), 5809–5812 (2018).

31. G.-W. Truong, E. M. Waxman, K. C. Cossel, E. Baumann, A. Klose, F. R. Giorgetta, W. C. Swann, N. R. Newbury, and I. Coddington, "Accurate frequency referencing for fieldable dual-comb spectroscopy," Opt. Express **24**(26), 30495–30504 (2016).

32. L. C. Sinclair, J.-D. Deschênes, L. Sonderhouse, W. C. Swann, I. H. Khader, E. Baumann, N. R. Newbury, and I. Coddington, "Invited Article: A compact optically coherent fiber frequency comb," Rev. Sci. Instrum. **86**(8), 081301 (2015).

33. S. Coburn, C. B. Alden, R. Wright, K. Cossel, E. Baumann, G.-W. Truong, F. Giorgetta, C. Sweeney, N. R. Newbury, K. Prasad, I. Coddington, and G. B. Rieker, "Regional trace-gas source attribution using a field-deployed dual frequency comb spectrometer," Optica **5**(4), 320–327 (2018).

34. G. Ycas, F. R. Giorgetta, E. Baumann, I. Coddington, D. Herman, S. A. Diddams, and N. R. Newbury, "High-coherence mid-infrared dual-comb spectroscopy spanning 2.6 to 5.2 μm," Nat. Photonics **12**(4), 202–208 (2018).

35. I. E. Gordon, L. S. Rothman, C. Hill, R. V. Kochanov, Y. Tan, P. F. Bernath, M. Birk, V. Boudon, A. Campargue, K. V. Chance, B. J. Drouin, J.-M. Flaud, R. R. Gamache, J. T. Hodges, D. Jacquemart, V. I. Perevalov, A. Perrin, K. P. Shine, M.-A. H. Smith, J. Tennyson, G. C. Toon, H. Tran, V. G. Tyuterev, A. Barbe, A. G. Császár, V. M. Devi, T. Furtenbacher, J. J. Harrison, J.-M. Hartmann, A. Jolly, T. J. Johnson, T. Karman, I. Kleiner, A. A. Kyuberis, J. Loos, O. M. Lyulin, S. T. Massie, S. N. Mikhailenko, N. Moazzen-Ahmadi, H. S. P. Müller, O. V. Naumenko, A. V. Nikitin, O. L. Polyansky, M. Rey, M. Rotger, S. W. Sharpe, K. Sung, E. Starikova, S. A. Tashkun, J. V. Auwera, G. Wagner, J. Wilzewski, P. Wcisło, S. Yu, and E. J. Zak, "The HITRAN2016 molecular spectroscopic database," J. Quant. Spectrosc. Radiat. Transf. **203**, 3–69 (2017).

36. C. D. Boone, K. A. Walker, and P. F. Bernath, "Speed-dependent Voigt profile for water vapor in infrared remote sensing applications," J. Quant. Spectrosc. Radiat. Transf. **105**(3), 525–532 (2007).

37. N. R. Newbury, I. Coddington, and W. Swann, "Sensitivity of coherent dual-comb spectroscopy," Opt. Express **18**(8), 7929–7945 (2010).

38. A. Klose, G. Ycas, D. L. Maser, and S. A. Diddams, "Tunable, stable source of femtosecond pulses near 2 μm via supercontinuum of an Erbium mode-locked laser," Opt. Express **22**(23), 28400–28411 (2014).

39. S. Wang, S. Droste, L. C. Sinclair, I. Coddington, N. R. Newbury, T. F. Carruthers, and C. R. Menyuk, "Wake mode sidebands and instability in mode-locked lasers with slow saturable absorbers," Opt. Lett. **42**(12), 2362–2365 (2017).

40. The use of tradenames in this manuscript is necessary to specify experimental results and does not imply endorsement by the National Institute of Standards and Technology.